



HAL
open science

Hydride-containing 2-Electron Pd/Cu Superatoms as Catalysts for Efficient Electrochemical Hydrogen Evolution

Rhone P. Brocha Silalahi, Yongsung Jo, Jian-Hong Liao, Tzu-Hao Chiu, Eunsaem Park, Woojun Choi, Hao Liang, Samia Kahlal, Jean-Yves Saillard, Dongil Lee, et al.

► **To cite this version:**

Rhone P. Brocha Silalahi, Yongsung Jo, Jian-Hong Liao, Tzu-Hao Chiu, Eunsaem Park, et al.. Hydride-containing 2-Electron Pd/Cu Superatoms as Catalysts for Efficient Electrochemical Hydrogen Evolution. *Angewandte Chemie International Edition*, 2023, pp.e202301272. 10.1002/anie.202301272 . hal-04013808

HAL Id: hal-04013808

<https://hal.science/hal-04013808>

Submitted on 30 Mar 2023

HAL is a multi-disciplinary open access archive for the deposit and dissemination of scientific research documents, whether they are published or not. The documents may come from teaching and research institutions in France or abroad, or from public or private research centers.

L'archive ouverte pluridisciplinaire **HAL**, est destinée au dépôt et à la diffusion de documents scientifiques de niveau recherche, publiés ou non, émanant des établissements d'enseignement et de recherche français ou étrangers, des laboratoires publics ou privés.



Distributed under a Creative Commons Attribution - NonCommercial 4.0 International License

Hydride-containing 2-Electron Pd/Cu Superatoms as Catalysts for Efficient Electrochemical Hydrogen Evolution

Rhone P. Brocha Silalahi,^[a] Yongsung Jo,^[b] Jian-Hong Liao,^[a] Tzu-Hao Chiu,^[a] Eunsuem Park,^[b] Woojun Choi,^[b] Hao Liang,^[c] Samia Kahlal,^[c] Jean-Yves Saillard,^{*,[c]} Dongil Lee,^{*,[b]} and C. W. Liu^{*,[a]}

[a] Dr. R. P. B. Silalahi, Dr. J.-H. Liao, T.-H. Chiu, Prof. Dr. C. W. Liu
Department of Chemistry
National Dong Hwa University
No. 1, Sec. 2, Da Hsueh Rd. Shoufeng, Hualien 97401 (Taiwan R. O. C.)
E-mail: chenwei@gms.ndhu.edu.tw

[b] Y. Jo, E. Park, Dr. W. Choi, Prof. Dr. D. Lee
Department of Chemistry
Yonsei University
Seoul 03722, Republic of Korea

[b] H. Liang, Dr. S. Kahlal, Prof. Dr. J.-Y. Saillard
Univ Rennes, CNRS, ISCR-UMR 6226
F-35000 Rennes, France

[+] These authors contributed equally to this work.

Supporting information for this article is given via a link at the end of the document.

Abstract: The first hydride-containing 2-electron palladium/copper alloys, $[\text{PdHCu}_{11}\{\text{S}_2\text{P}(\text{O}^i\text{Pr})_2\}_6(\text{C}\equiv\text{CPh})_4]$ (**PdHCu₁₁**) and $[\text{PdHCu}_{12}\{\text{S}_2\text{P}(\text{O}^i\text{Pr})_2\}_5\{\text{S}_2\text{PO}(\text{O}^i\text{Pr})\}_1(\text{C}\equiv\text{CPh})_4]$ (**PdHCu₁₂**), are synthesized from the reaction of $[\text{PdH}_2\text{Cu}_{14}\{\text{S}_2\text{P}(\text{O}^i\text{Pr})_2\}_6(\text{C}\equiv\text{CPh})_6]$ (**PdH₂Cu₁₄**) with trifluoroacetic acid (TFA). X-ray diffraction reveals that the **PdHCu₁₁** and **PdHCu₁₂** kernels consist of a central PdH unit encapsulated within a vertex-missing Cu₁₁ cuboctahedron and complete Cu₁₂ cuboctahedron, respectively. DFT calculations indicate that both **PdHCu₁₁** and **PdHCu₁₂** can be considered as axially-distorted 2-electron superatoms. **PdHCu₁₁** shows excellent HER activity, unprecedented within metal nanoclusters, with an onset potential of -0.05 V (at 10 mA cm⁻²), a Tafel slope of 40 mV dec⁻¹, and consistent HER activity during 1000 cycles in 0.5 M H₂SO₄. Our study suggests that the accessible central Pd site is the key to HER activity and may provide guidelines for correlating catalyst structures and HER activity.

Introduction

The use of hydrogen in sustainable energy technologies, such as fuel cells and solar fuel generators, has sparked a lot of attention. The creation of low-cost hydrogen sources remains difficult.^{1,2} The most advantageous method for obtaining renewable hydrogen generation is thought to be *via* the hydrogen evolution reaction (HER).³ A useful electrocatalyst with high stability, durability, and hydrogen generation efficiency requirements is the most difficult part of the HER process.^{4,5} Metal catalysts, especially those based on platinum, dominate HER but still have challenges in achieving stable hydrogen generation over the long term because of their high prices and volatility.⁶ Palladium, like platinum, possesses exceptional qualities that allow it to display great electrocatalytic activity because of its capacity to absorb significant volumes of hydrogen under ambient settings.^{7,8} Cu has been identified as a key player in increasing catalytic characteristics through a synergistic impact in Pd-based alloy electrocatalysts.⁹ As a

result, Pd-Cu nanoalloys have been the subject of in-depth study as fuel cell electrocatalysts.¹⁰⁻¹² In the current work, doping copper-hydride precursors with palladium to create hydride-bridged Pd-Cu alloys will be investigated in an effort to find a novel electrocatalyst for HER.

Recently, bimetallic catalysts gained more attention due to their properties which can be easily tuned, enabling catalytic activity that generally cannot be accessed or mimicked by monometallic species. Moreover, it may be possible to design a bimetallic catalyst based on earth-abundant elements only and can still be effective for HER.¹³ However, creating a superatomic bimetallic alloy cluster as an active HER catalyst is still uncommon. A notable example is the 6-electron, bimetallic nanocluster PtAu₂₄(SC₆H₁₃)₁₈, which exhibits supreme HER performance, even better than benchmarking platinum catalysts.¹⁴ Nevertheless, the scarcity and high price of these noble metals hinder their commercial use.

We have developed a method of doping dichalcogenolates-stabilized copper hydrides. Reactions of polyhydrido copper clusters $[\text{Cu}_{28}\text{H}_{15}(\text{dte})_{12}]^{+}$,¹⁵ or $[\text{Cu}_{20}\text{H}_{11}(\text{dtp})_9]^{16}$ with a Pd(II) salt in the presence of phenylacetylene produce $[\text{PdH}_2\text{Cu}_{14}(\text{dte}/\text{dtp})_6(\text{C}\equiv\text{CPh})_6]$ (dte = di-butyl dithiocarbamate; dtp = di-isopropyl dithiophosphate).¹⁷ In these clusters, the 14 Cu(I) atoms feature a *D_{3d}* bicapped icosahedron enclosed a linear 14-e $[\text{PdH}_2]^{2-}$ unit. Recent findings on hydride-doped noble metal nanoclusters clearly indicate that the hydride is a component of the superatom core.¹⁸ To the best of our knowledge, only a few examples of nanoclusters containing encapsulated hydrides have been reported.¹⁸⁻²⁰ Most of them are 8-electron *superatoms*, the electron of the encapsulated hydrogen contributing to this count. Both $[\text{PtHAg}_{19}(\text{dtp}/\text{desp})_{12}]$ (dtp = $\text{S}_2\text{P}(\text{O}^i\text{Pr})_2$; desp = $\text{Se}_2\text{P}(\text{O}^i\text{Pr})_2$)¹⁸ and $[\text{RhHAg}_{24}(\text{SPhMe}_2)_{18}]^{2-}$,¹⁹ exhibit an MH-centered icosahedral core, $[\text{PtH@Ag}_{12}]^{5+}$ and $[\text{RhH@Ag}_{12}]^{4+}$, respectively. In the $[\text{HPdM}_2\text{Au}_8(\text{PMe}_3)_8\text{Cl}_2]^+$ (M = Ag, Cu) species, the H atom is thought to bridge a Pd-Au vector in the $(\text{HPd@M}_2\text{Au}_8)^{3+}$ *superatomic* core.²⁰ On the other hand, no 2- *electron*

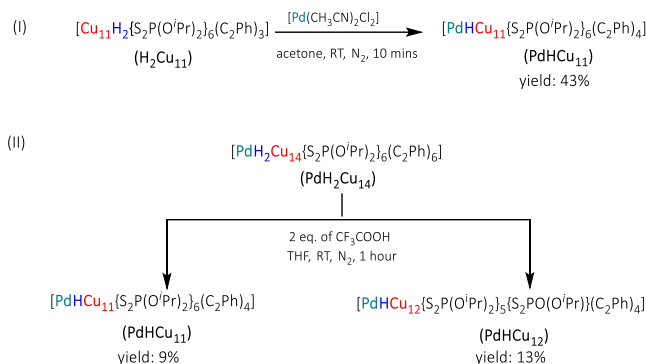
nanoclusters in which the hydride is a superatomic constituent have been reported so far.

Herein first hydride-containing 2-electron palladium/copper superatomic alloys co-protected by alkynyl and dithiophosphato ligands are prepared by the treatment of **PdH₂Cu₁₄**¹⁷ with trifluoroacetic acid (TFA). Structures of [PdHCu₁₁{S₂P(OⁱPr)₂}(C≡CPh)₄] (**PdHCu₁₁**), and [PdHCu₁₂{S₂P(OⁱPr)₂}(S₂PO(OⁱPr))(C≡CPh)₄] (**PdHCu₁₂**), are determined by single-crystal X-ray diffraction (SC-XRD), and their compositions are further confirmed by electrospray ionization mass spectrometry (ESI-MS). The new **PdHCu₁₁** shows a metal framework consisting of a Pd(0) atom at its center, surrounded by a vertex-missing Cu₁₁ cuboctahedron. **PdHCu₁₂** can be viewed as a complete Pd-centered Cu₁₂ cuboctahedron. The hydride in both **PdHCu₁₁** and **PdHCu₁₂** is located within a tetrahedral PdCu₃ cavity. Electrochemical HER experiments indicate that **PdHCu₁₁**, **PdHCu₁₂**, and **PdH₂Cu₁₄** are active catalysts, but the stability and efficiency of **PdHCu₁₁** are much higher than those of **PdHCu₁₂** and **PdH₂Cu₁₄**. The high HER activity of **PdHCu₁₁** is likely attributed to the open PdH unit inside the defective Cu₁₁ cuboctahedron that acts as an active site for hydrogen production.

Results and Discussion

In a typical synthesis, one equiv. [Cu₁₁H₂{S₂P(OⁱPr)₂}(C≡CPh)₃}²¹ (**H₂Cu₁₁**) was firstly dissolved in acetone, and then an equimolar amount of [Pd(CH₃CN)₂Cl₂] was added instantaneously. The reaction was stirred at room temperature for 10 minutes under N₂. Dark residues after solvent removal were washed with a hexane/water mixture. The hexane layer was separated and dried under vacuum to yield [PdHCu₁₁{S₂P(OⁱPr)₂}(C≡CPh)₄] in 43% yield (Scheme 1). Its deuterated derivative [PdDCu₁₁{S₂P(OⁱPr)₂}(C≡CPh)₄] (abbreviated **PdDCu₁₁**) was synthesized to support the presence of the hydride ligand by reacting equimolar amounts of [Cu₁₁D₂{S₂P(OⁱPr)₂}(C≡CPh)₃] and [Pd(CH₃CN)₂Cl₂] in 34% yield. The two hydrides in the **H₂Cu₁₁** template appear to behave simultaneously as reductants and Lewis bases, reducing Pd(II) to Pd(0) and supplying the hydride ligand in **PdHCu₁₁**.^{22,23} Presumably, an aggregation occurs during the reaction, which leads to the addition of one alkynyl ligand in the yielded alloy cluster. Alternatively, **PdHCu₁₁** can also be synthesized by the addition of two equiv. of CF₃COOH to **PdH₂Cu₁₄** at room temperature in ~9%. In the same reaction, another 2-electron Pd-Cu alloy cluster, [PdHCu₁₂{S₂P(OⁱPr)₂}(S₂PO(OⁱPr))(C≡CPh)₄] (abbreviated **PdHCu₁₂**), was generated in 13% yield (Scheme 1). Its deuterated derivative [PdDCu₁₂{S₂P(OⁱPr)₂}(S₂PO(OⁱPr))(C≡CPh)₄] (abbreviated **PdDCu₁₂**), was also synthesized. The acid addition provokes the peeling away of two units of CuC≡CPh, one CuH to reach the formation of **PdHCu₁₁**, and unexpected acid-induced de-esterification of [S₂P(OⁱPr)₂]⁻ (O, O'-diisopropylidithiophosphato-S, S') to form a di-negative charge [S₂PO(OⁱPr)]²⁻ (O-isopropylidithiophosphato-S, S') ligand in **PdHCu₁₂** (Scheme S1). Both **PdHCu₁₁** and **PdHCu₁₂** can be easily separated by solvents.

The composition of **PdHCu₁₁** was first determined by positive-ion electrospray ionization mass spectrometry (ESI-MS).



Scheme 1. Synthetic pathways of **PdHCu₁₁** by using (I) the **H₂Cu₁₁** template and (II) the acid treatments on **PdH₂Cu₁₄** to afford **PdHCu₁₁** and **PdHCu₁₂**.

Figure S1a shows an intense mass peak at m/z 2554.22 Da (calcd. 2554.32 Da), corresponding to the adduct cation of **[PdHCu₁₁+Cu]⁺**. The theoretical isotopic pattern of **[PdHCu₁₁+Cu]⁺** shows a great resemblance to the experimental one (Figure S1b). The ESI-MS spectrum of **PdDCu₁₁** shows a fragment peak at m/z 2391.37 Da, corresponding to degradation of **PdDCu₁₁** via loss of one phenyl acetylde, **[PdDCu₁₁-(C≡CPh)]⁺** (calc. 2389.36 Da). Both simulated and experimental isotopic patterns match well (Figure S2 and inset). The ¹H and ¹³C NMR spectroscopy analyses of **PdHCu₁₁** show one set of isopropyl groups and phenyl ring corresponding to the dtp and alkynyl ligands (Figures S3 and S4). The hydride in **PdHCu₁₁** displays a single peak at 3.69 ppm in *d*₆-acetone. Its deuteride analogue, **PdDCu₁₁**, appears at 3.46 ppm in acetone (Figures S5 and S6). The ³¹P{¹H} NMR spectrum reveals the presence of six resonances for **PdHCu₁₁** (93.4, 95.9, 98.8, 100.2, 101.9 and 103.9 ppm), which are significantly shifted up-field in comparison with that of the **H₂Cu₁₁** (104.1 ppm) template (Figures S7 and S8). The spectral pattern suggests that going from the **H₂Cu₁₁** template to the **PdHCu₁₁** alloy yields structural changes from C₃ to C₁ symmetry.

The composition of **PdHCu₁₂** was verified by ESI-MS analysis (Figures S1c and S9). A less-intense peak identified at m/z = 2512.1038 Da (calcd. 2510.2734 Da) can be assigned as the parent species, **PdHCu₁₂**. In addition, a prominent peak at m/z at 2574.02 Da is the adduct ion **[PdHCu₁₂+Cu]⁺** (calcd. 2573.20 Da). Their accuracy was further verified by isotope analysis, where both experimental and simulated isotopic patterns of **PdHCu₁₂** and **[PdHCu₁₂+Cu]⁺** are in perfect agreement. The ESI-MS spectrum of **PdDCu₁₂** shows a fragment peak at m/z 2413.99 Da (calcd. 2411.22 Da), corresponding to **PdDCu₁₂** with a loss of one phenyl acetylde (Figure S10). The ¹H NMR spectrum of **PdHCu₁₂** depicts one set of C≡CPh, two sets of isopropyl groups corresponding to five one-negative charge dtp ligands, and one set of isopropyl groups of [S₂P(O)(OⁱPr)]²⁻ ligands (Figure S11). While the chemical shifts of -CH and -CH₃ in dtp ligands appear at 4.96 and 1.09 ppm, the corresponding protons in [S₂PO(OⁱPr)]²⁻ resonate at 4.54 and 0.62 ppm with the integration ratio of [S₂P(OⁱPr)₂]⁻ and [S₂PO(OⁱPr)]²⁻ closed to 10:1. The hydride in **PdHCu₁₂** displays a single peak at -5.19 ppm in *d*₆-acetone. Its deuteride analogue, **PdDCu₁₂**, appears at -4.98 ppm in chloroform (Figures S12 and S13). The hydride resonance in the

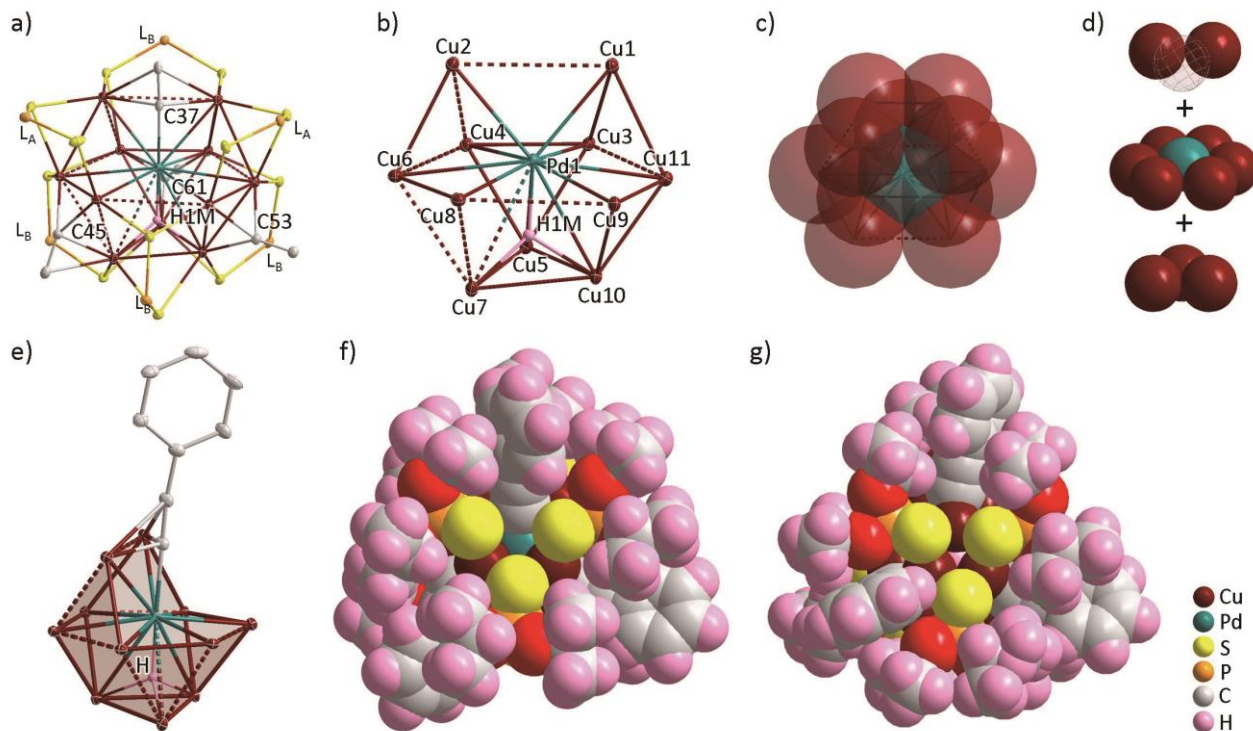


Figure 1. a) The structure of **PdHCu₁₁**. Phenyl groups and iso-propoxy groups are omitted for clarity. b) The **PdHCu₁₁** core. c) The defective cuboctahedron. d) A schematic representation of the defect in the *fcc* arrangement. e) The unique μ_3 : η^1 , η^2 , η^2 binding fashion of one phenyl acetylide. f) The space-filling model of **PdHCu₁₁**, which is viewed down the vacant site, g) and normal site.

Cu₁₁ shell that describes a defective copper cuboctahedron (**PdHCu₁₁**) is shifted downfield compared to the hydride in the **Cu₁₂** shell, a cuboctahedron (**PdHCu₁₂**). The pattern of ¹³C NMR in **PdHCu₁₁** was observed in **PdHCu₁₂** (Figure S14). The ³¹P{¹H} NMR spectrum of dtp and [S₂PO(O'Pr)]²⁻ ligands in **PdHCu₁₂** shown in Figure S15 displays peaks centered at 101.4, 100.4, 97.1, 96.9, and 92.1 ppm attributed to the phosphorus nuclei in dtp ligands, and a peak centered at 66.7 ppm, which can be reasonably assigned as the chemical shift of [S₂PO(O'Pr)]²⁻ (Figure S15). The spectral pattern suggests that the **PdHCu₁₂** alloy has *C₁* symmetry.

The photoelectron spectroscopic studies have been used to evaluate the metal oxidation states. The Pd 3d spectra and their peak positions from the **PdHCu₁₁** and **PdHCu₁₂** are shown in Figure S16. The XPS analysis of **PdHCu₁₁** indicates binding energy at 336.7 and 342.3 eV, corresponding to Pd(0) 3d_{5/2} and 3d_{3/2}, respectively (Figure S16a). Peaks are also detected at 336.9 and 341.9, respectively, corresponding to the 3d_{5/2} and 3d_{3/2} electronic states of Pd(0) species in **PdHCu₁₂** (Figure S16b). These values are slightly higher than the Pd(0) 3d_{5/2} (336.0 eV) and 3d_{3/2} (341.0 eV) observed in [PdH₂Cu₁₄{S₂CNⁿBu₂}₆(C≡CPh)₆].¹⁷ The element contents of **PdHCu₁₁** and **PdHCu₁₂** from XPS fit exactly with the existence of the expected elements (Figures S17 and S18).

Single-crystal X-ray crystallography (SC-XRD) analysis reveals that the kernel of **PdHCu₁₁** consists of a Pd-centered **Cu₁₁** skeleton with one interstitial hydride, protected by six dtp and four alkynyl ligands (Figure 1a). The Cu atoms occupy eleven among the twelve vertices of a cuboctahedron (Figure 1b), thus leaving one vertex vacant (represented by □). The twelve metal atoms (Pd@[Cu₁₁□]) are distributed in three layers

by atomic ratios of 2:7:3, where one Cu atom is missing on the vacancy-containing top layer (Figure 1c and 1d), thus describing a defective face-centered cubic metal array. A similar defect in [AuCu₁₁{S₂P(O'Pr)₂}(C≡CPh)₃Cl] (**AuCu₁₁**) was reported recently.²² These defective structures are related to a complete centered-cuboctahedral (ideal *fcc*) arrangements M@Cu₁₂ existing in the [MCu₁₂{dtc/dtp}₆(C≡CPh)₆]⁺ (M = Cu, Ag, Au) clusters.^{24,25} The Cu...Cu separations (2.6974(6) Å–3.4624(8) Å) in **PdHCu₁₁** are distributed in a wider range than those in **AuCu₁₁** (2.5319(15)–3.212(2) Å), indicating that the former has a larger degree of distortion. The longest Cu...Cu separation (3.4624(8) Å) in **PdHCu₁₁** lies between Cu1 and Cu2 (Figure 1b) due to the intrusion of one alkynyl ligand on top of the Pd@[Cu₁₁□] vacant site. This contrasts with **AuCu₁₁**, where the bridging chloride ligand stays on the surface. The Pd-Cu distances in **PdHCu₁₁** (avg. 2.8411(5) Å) are longer than in **PdH₂Cu₁₄** (avg. 2.741(7) Å).¹⁷ The Pd1...Cu7 separation (3.0677(5) Å) is beyond the sum of van der Waals radii (1.63+1.40 = 3.03 Å), reflecting the nature of the defective cuboctahedron. *The hydride atom was located from the Fourier maps and refined freely without constraint.* It is situated on the axis defined by the central Pd and the intruded alkyne but opposite the vacancy, occupying a tetrahedral cavity defined by Pd and a Cu₃ face of the defective cuboctahedron. The average Cu-H distance is 1.77(4) Å, and the Pd-H distance (1.69(4) Å) is slightly shorter than the Pd-H distance in [PdH₂Cu₁₄{S₂CNⁿBu₂}₆(C≡CPh)₆] (1.759(14) Å, neutron data).¹⁷ DFT calculations confirm this position, and its location opposite to the cluster open side appears to be the first one among those hydride-containing alloys where the hydride electron is a part of superatom electron count (*vide infra*).

The outer shell of **PdHCu₁₁** is covered by six dtp, and four alkynyl ligands, which are in the same positions as in **AuC₁₁**, except one additional alkynyl in **PdHCu₁₁** (on C37, Figure 2a) replaces the chloride ligand in **AuC₁₁**. The six dtp ligands can be grouped into two bridging modes, dtp_A (μ_1, μ_2) and dtp_B (μ_2, μ_2), due to the lack of one vertex in the cuboctahedron. The average Cu-S distance in the dtp_A bridging mode (2.2975(10) Å) is slightly shorter than in the dtp_B bridging mode (avg. 2.3490(10) Å). Four alkynyl ligands exhibit three different coordination modes, of which three are coordinated to the Cu₃ triangular faces of the defective cuboctahedron with two in $\mu_3: \eta^1, \eta^1, \eta^1$ coordination mode (ligands on C53 and C61) and one in a $\mu_3: \eta^1, \eta^1, \eta^2$ mode (ligand on C45). Because of the “missing” Cu, the fourth alkynyl ligand (on C37) is coordinated not only to two Cu atoms (Cu1 and Cu2) but also to the central Pd atom (Pd-C37 = 2.046(4) Å) in a unique $\mu_3: \eta^1, \eta^2, \eta^2$ fashion (Figure 1b and 1e). It shows both σ and π coordination modes through both C≡C carbons. Thus, this alkynyl ligand somewhat penetrates the metallic core because of a vacancy. *Being bonded on each side by the hydride and an alkynyl carbon, respectively, the Pd atom forms a quasi-linear H-Pd-C motif. PdHCu₁₁ is the first example of an alkynyl directly coordinated to a Pd(0)-H motif, to the best of our knowledge.*

The vacancy induces the intrusion of an alkynyl ligand and leads to the symmetry breaking from T_d in $M@Cu_{12}$ to C_1 in **PdHCu₁₁**. Despite the partial occupation of the vacancy by an alkynyl ligand, the void still exists. In the space-filling model of **PdHCu₁₁** (Figure 1f), the central Pd atom is clearly visible through viewing the vacant site. However, the central Pd atom is entirely shielded by Cu atoms and ligands viewed from the opposite orientation (Figure 1g). *Thus it can be assumed that the presence of this vacancy makes it easier for a reactant to penetrate and interact with the inner Pd(0) atom, thereby favoring the HER catalytic activity (see below).*

The structure of **PdHCu₁₂** comprises a Pd-centered Cu₁₂ cuboctahedron with an interstitial hydride, six dtp ligands, and four alkynyl ligands (Figure 2a). The metal array in **PdHCu₁₂** exhibits a non-defect fcc stacking, constituting a distorted cuboctahedron with 24 Cu...Cu separations in a range of 2.5654(12)-3.542(1) Å. The central Pd atom shows short contacts with eleven adjacent Cu atoms (avg. 2.8443(11) Å). A long Pd1...Cu12 distance of 3.039(1) Å is found slightly beyond the sum of their van der Waals radii. Each dtp ligand bridges to the square face of the cuboctahedron in (μ_2, μ_2) coordination mode. Interestingly, one of the dtp ligands underwent a C-O bond cleavage, forming [S₂PO(O'Pr)]²⁻. The P2-O4 distance of 1.503(6) Å, which was identified as a P=O bond in the [S₂PO(O'Pr)]²⁻ ligand, is significantly shorter than the P2-O3 single bond (1.604(7) Å). Each alkynyl ligand bridges onto a triangular face of the Cu₁₂ cuboctahedron through a $\mu_3: \eta^1, \eta^1, \eta^1$ fashion with averaged C-Cu distance of 2.034(8) Å. However, one of them (containing C58, see Figure 2b) penetrates the Cu₁₂ cuboctahedron, expanding the Cu1-Cu2-Cu3 triangular face, causing large Cu...Cu separations (3.481(1), 3.495(1), and 3.542(1) Å). Thus, C58 is bonded to Cu1, Cu2 and Cu3, as well as to the central Pd atom (C58-Pd1: 2.11(8) Å). The interstitial hydride (H1M) was located from the residual densities and refined without any constraints. Its location is near-identical to **PdHCu₁₁**, showing a quasi-linear C58-Pd1-H1M unit. The Cu-H (avg. 1.80(7) Å) and the Pd-H distances (1.70(6) Å) in **PdHCu₁₂** are similar to those in **PdHCu₁₁**. In the space-filling model of

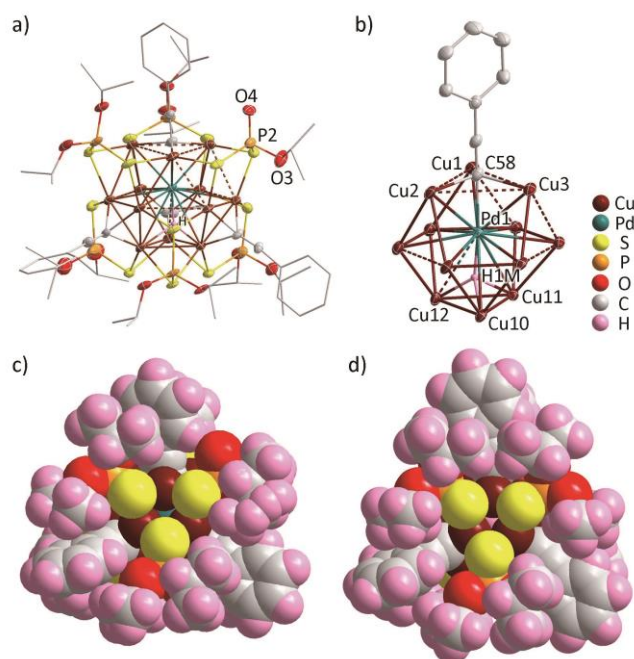


Figure 2. a) The total structure of **PdHCu₁₂**. b) PdH@Cu₁₂ framework with a penetrated alkynyl ligand. c) The space-filling model of **PdHCu₁₂**, viewed down the expanded Cu₃ triangular face, and d) viewed down the interstitial hydride.

PdHCu₁₂, the central Pd atom is barely visible due to being highly shielded by the twelve Cu atoms (Figure 2c), and the interstitial hydride remains in a similar confined environment as in **PdHCu₁₁** (Figure 2d).

Density functional theory (DFT) calculations have been carried out at the PBE0/Def2TZVP level (see Computational Details section) on simplified models (**PdHCu₁₁'** and **PdHCu₁₂'**) in which the S₂P(O'Pr)₂ and S₂PO(O'Pr) ligands were replaced by S₂PH₂ and S₂PO(H), respectively, in order to reduce computational cost. Selected computed data are given in Table 1. The optimized geometry of **PdHCu₁₁'** is found to be in good agreement with the X-ray structure of **PdHCu₁₁**. In particular, it fully confirms the position of the hydride in the PdCu₃ tetrahedron *opposite to the cuboctahedron vacancy*. Its position within the tetrahedron is found to be quite symmetrical (H-Cu range: 1.781-1.806 Å), with a shorter Pd-H distance. Consistently, the Pd-H Wiberg bond index is significantly larger than the Cu-H ones (Table 1), indicating much stronger Pd-H bonding.

The Kohn-Sham MO diagram of **PdHCu₁₁'** is shown on the left side of Figure 3. Its HOMO is of dominant Pd character (35%) with ~3-4% participation on each Cu. Owing to the important contribution of the metal valence s (and, to a lesser extent, p) AOs in this HOMO and its spheroidal shape, it can be identified as a *superatomic* 1S orbital. It is actually quite similar to the 1S HOMO of the structurally related **AuC₁₁**,²² and by consequence to the HOMO of the ideally cuboctahedral [MCu₁₂(dtc/dtp)₆(C≡CPh)₆]⁺ (M = Cu, Ag, Au) clusters.^{24,25} Considering all these species as being 2-electron *superatoms* with 1S² 1P⁰ configuration stresses the role of the encapsulated hydride in **PdHCu₁₁**. Going from **AuC₁₁** to **PdHCu₁₁** corresponds to the formal isoelectronic replacements of Cl by C≡CPh and Au by PdH. Thus, the hydride electron contributes to the *superatom* electron count. Removing the encapsulated

Table 1. Selected experimental (X-ray) data for **PdHCu₁₁** and **PdHCu₁₂** and DFT-computed data for **PdHCu₁₁'** and **PdHCu₁₂'** (WBI = Wiberg bond index, NAO = natural atomic orbital).

Distance (Å)	PdHCu₁₁ (X-ray)	PdHCu₁₁' (DFT)	PdHCu₁₂ (X-ray)	PdHCu₁₂' (DFT)
Cu-Cu (av.)	2.7902(6)	2.810 [0.034]	2.823(1)	2.970 [0.027]
Pd-Cu (av.)	2.8411(5)	2.880 [0.040]	2.860(5)	2.902 [0.034]
Cu-S (av.)	2.3350(10)	2.371 [0.163]	2.318(6)	2.356 [0.175]
Cu-C (av.)	2.028(4)	2.041 [0.170]	2.037(4)	2.049 [0.170]
Pd-C	2.046(4)	2.044 [0.372]	2.110(0)	2.095 [0.318]
Pd-H	1.70(4)	1.678 [0.303]	1.613(8)	1.681 [0.317]
Cu-H (av.)	1.77(4)	1.791 [0.061]	1.844(8)	1.816 [0.059]
NAO charges				
Cu (av.)		0.76		0.74
Pd		-0.47		-0.43
H (hydride)		-0.54		-0.53

hydrogen in **PdHCu₁₁'** as a proton generates the 2-electron *superatom* [**PdCu₁₁(S₂PH₂)₆(C≡CPh)₄**], the optimized structure of which is quite similar to that of **PdHCu₁₁'** (see SI). Replacing, in this latter cluster, the C≡CPh ligand connected to Pd by Cl generates a 2-electron cluster very similar to the known **AuCu₁₁**.²² Among these two anionic models of 1S² 1P⁰ configuration, the latter has its 1P_x, 1P_y and 1P_z orbitals close in energy and lying among the lowest unoccupied levels, as for **AuCu₁₁**²² and the [MCu₁₂(dtp/dtp)₆(C≡CPh)₆]⁺ (M = Cu, Ag, Au) clusters.^{24,25} This is not the case for the former model [**PdCu₁₁(S₂PH₂)₆(C≡CPh)₄**], for which the 1P_z orbital (z-axis along the Pd-C bond) is found higher in energy due to its destabilization by the C≡CPh ligand. In the case of **PdHCu₁₁**, only the 1P_x (LUMO) and 1P_y (LUMO+1) orbitals could be clearly identified (Figure 3). In fact, the missing 1P_z orbital is now involved in the bonding with both a C≡CPh ligand and the encapsulated hydride. Thus, **PdHCu₁₁** should be better viewed as an *axially-distorted 2-electron superatom*. On the other hand, the related **AuCu₁₁** remains a fairly pseudo-spherical *superatom*, despite its missing vertex. It is worth mentioning that the 1s electrons of the hydrides in [AuCu₂₄H₂₂(PPh₃)₁₂]⁺,²⁶ a 2-e superatomic alloy, do not contribute to the *superatom* electron count.

In the recently characterized 8-electron [PtHAg₁₃(dtp/desp)₁₂] (dtp = S₂P(OⁿPr)₂; desp = Se₂P(OⁿPr)₂),¹⁸ the encapsulated hydride does not participate significantly in the

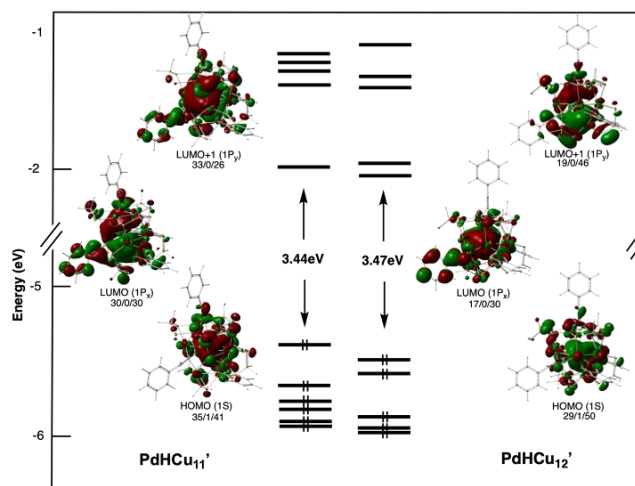


Figure 3 Kohn-Sham orbital diagrams of **PdHCu₁₁'** and **PdHCu₁₂'**. Orbital localization (in %) is given in the order Pd/H/Cu₁₁.

building of the *superatomic* orbitals but interacts principally with the 5d_{z²}(Pt) orbital to form a kind of Pt-H σ bond. In spite of its particularly low symmetry, which tends to blur orbital analyses, a more or less similar situation can be traced for **PdHCu₁₁'**, for which the simplified MO diagram sketched in Scheme S2 can be proposed. Thus, going from **AuCu₁₁** to **PdHCu₁₁** corresponds to the replacement of Au by an isoelectronic PdH unit, associated with a substantial axial (H-Pd-C) distortion, to which the substitution of Cl (in **AuCu₁₁**) by CPh (in **PdHCu₁₁'**) is also contributing. Though a couple of hydride-doped gold-rich nanoclusters in which the hydrogen electron also contributes to the *superatom* electron count have been reported,²⁷ **PdHCu₁₁** is the first example in which the hydride is not located near the open side of the cage but rather on the opposite side.

The optimized geometry of **PdHCu₁₂'** is also found to match that of its X-ray counterpart (Table 1), including with respect to the hydride location. Its electronic structure is strongly related to that of **PdHCu₁₁'** (Table 1 and Figure 3). Similar to **PdHCu₁₁'**, it is an axially-distorted 2-electron *superatom* with 1S² 1P⁰ configuration. The strong parentage between **PdHCu₁₁'** and **PdHCu₁₂'** supports the view that the *superatom* model can be safely applied to clusters with incomplete external metal spheres, such as the defective cuboctahedra existing in **AuCu₁₁** or **PdHCu₁₁'**. This parentage reminds the *nido/closo* relationships in the Wade-Mingos clusters.²⁸ Finally, it can be noted that TD-DFT calculations on **PdHCu₁₁'** and **PdHCu₁₂'** reproduce satisfyingly the shapes of the **PdHCu₁₁** and **PdHCu₁₂** UV-vis spectra (Figure S19), with a low-energy band assigned to a HOMO→LUMO transition.

The HER activity of the open-structured Pd-doped Cu nanocluster, **PdHCu₁₁**, was examined by linear sweep voltammetry (LSV) in a three-electrode electrochemical cell containing 0.5 M H₂SO₄ (see Experimental Section for details). To investigate the structural effect on the HER activity, the HER activity of **PdHCu₁₁** was compared with those of **PdHCu₁₂** and **PdH₂Cu₁₄**. The nanocluster-immobilized working electrodes were fabricated by dropcasting a cluster solution onto a carbon paper (**PdHCu₁₁/C**, **PdHCu₁₂/C** and **PdH₂Cu₁₄/C**). Figure 4a shows the LSVs of **PdHCu₁₁/C**, **PdHCu₁₂/C** and **PdH₂Cu₁₄/C** in Ar saturated 0.5 M H₂SO₄ solution. As shown in Figure 4a, the **PdHCu₁₁** exhibits much higher HER activity than **PdHCu₁₂** and

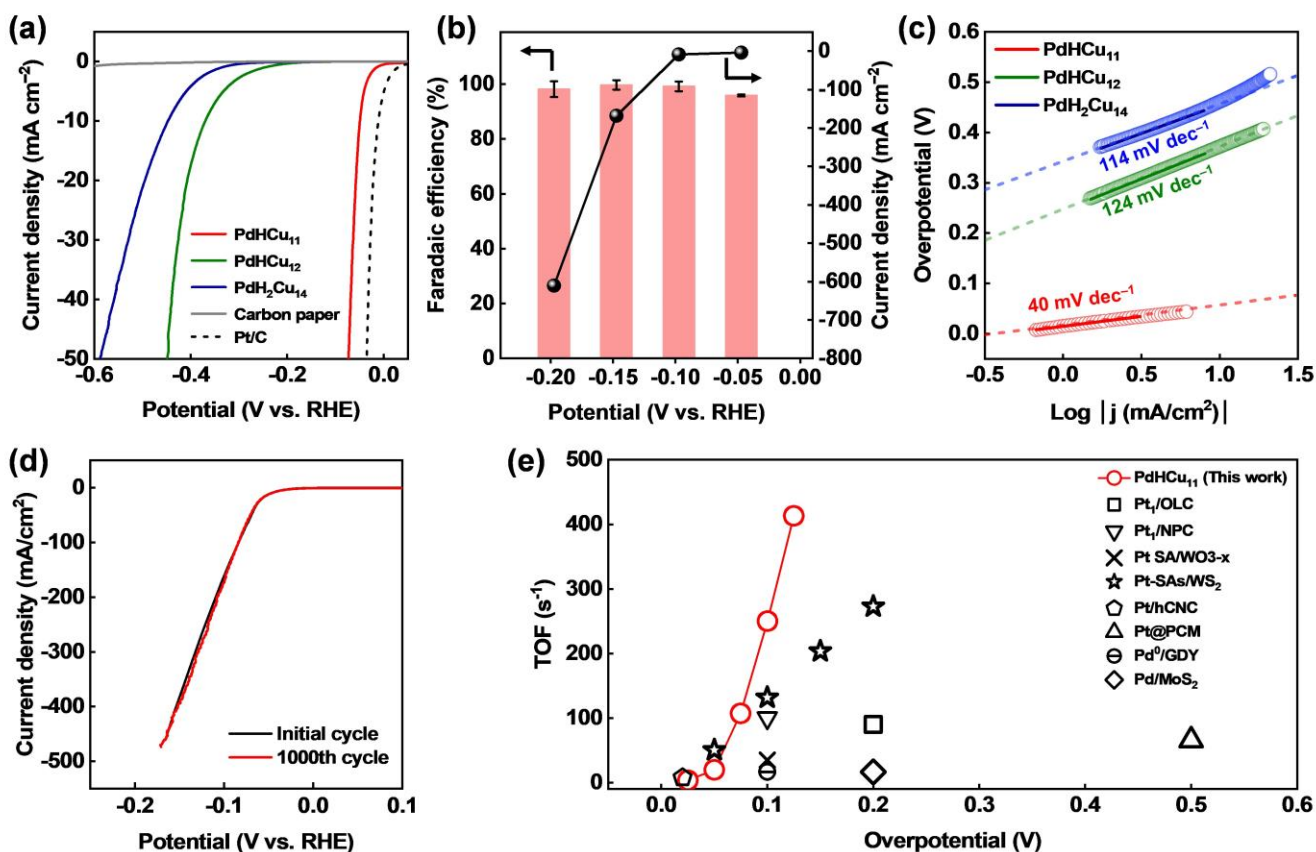


Figure 4. a) LSVs recorded at 1 mV s⁻¹ on PdHCu₁₁/C, PdHCu₁₂/C, PdH₂Cu₁₄/C, Pt/C, and carbon paper. b) Faradaic efficiencies and current densities for H₂ production measured for PdHCu₁₁/C at various applied potentials. c) Tafel plots for HER on PdHCu₁₁/C, PdHCu₁₂/C, and PdH₂Cu₁₄/C. d) Cyclic voltammograms recorded at 50 mV s⁻¹ on PdHCu₁₁/C during 1000 cycles. All measurements in (a)-(d) were conducted in Ar-saturated solution of 0.5 M H₂SO₄. e) Comparison of TOF values for H₂ production determined for PdHCu₁₁ (red circles) with other electrocatalysts (Table S2). All potentials were iR-corrected.

PdH₂Cu₁₄ nanoclusters; the HER onset potential for PdHCu₁₁ was observed at ~0.0 V vs. reversible hydrogen electrode (RHE), which was close that of the benchmark Pt/C (20 wt.%) catalyst. [Hereafter, all potentials are reported vs. RHE unless noted otherwise.] Note that the HER activity of the carbon paper was negligible as compared in Figure 4a. The overpotentials for the current density of 10 mA cm⁻² were found to be -0.05, -0.37 and -0.45 V for PdHCu₁₁, PdHCu₁₂ and PdH₂Cu₁₄, respectively, indicating that PdHCu₁₁ is a more efficient H₂-producing electrocatalyst. To determine the current efficiency for H₂ production, controlled potential electrolysis (CPE) measurements were conducted in an H-cell, and the produced gas was analyzed by gas chromatography (see Experimental Section). As can be seen in Figure 4b, the faradaic efficiency for H₂ was found to be 96 % at -0.05 V and increased to over 99 % when the potential was -0.10 V and below, indicating that the current was exclusively used for H₂ production.

To identify the origin of the vastly different HER activities observed for these nanoclusters, Tafel analyses were conducted in a kinetically controlled regime. Figure 4c shows that the Tafel slope obtained for PdHCu₁₁ is dramatically different from those obtained for PdHCu₁₂ and PdH₂Cu₁₄, indicating that the HER occurs via distinctly different pathways on these nanoclusters. Whereas the sluggish kinetics (114–124 mV dec⁻¹) suggests that the HER processes on both PdHCu₁₂ and PdH₂Cu₁₄ are limited by the Volmer step, the low Tafel slope (40 mV dec⁻¹) obtained for PdHCu₁₁ suggests that the HER occurs via the

Volmer–Heyrovsky pathway.²⁹ The distinctly different HER activity and kinetics observed for PdHCu₁₁ unambiguously confirm that the HER occurs via a distinctly different pathway, even though all Pd-Cu nanoclusters have the Pd dopant in the central position. Importantly, PdHCu₁₁ demonstrated high durability, exhibiting consistent HER activity during 1000 cycles (Figure 4d). ESI-MS analysis also confirmed that the PdHCu₁₁ catalyst maintained its structural integrity during the HER process (Figure S20). In Figure S21, PdHCu₁₁ showed a near-zero HER onset potential in 1.0 M KOH, but it exhibited more sluggish HER kinetics with a Tafel slope of 80 mV dec⁻¹ than that observed in 0.5 M H₂SO₄. This result indicates that the water dissociation step that precedes the HER process²⁹ is not effectively catalyzed by the open-structured PdHCu₁₁ in alkaline media.

PdHCu₁₁ can be considered as a Pd atom stabilized in a defective cuboctahedron allowing access of the reactant to the catalytic site. It is interesting to note that the TOF values obtained for PdHCu₁₁ are higher than most efficient single-atom catalysts, including Pt single-atom catalysts, under similar conditions (Figure 4e and Table S2). More specifically, compared to other bimetallic nanoclusters reported to be efficient HER electrocatalysts (Table S3),^{14,30-35} it is the one with the best activity. Evidently, the Pd atom in PdHCu₁₁ is fully utilized for H₂ production, presumably owing to its unique open structure. Another interesting aspect of the PdHCu₁₁ structure is the role of the hydride in the HER process. To probe this, we

retrieved the **PdHCu₁₁** catalyst after conducting electrolysis at –0.25 V for 2.5 h in 0.5 M D₂SO₄ and analyzed it using mass spectrometry. As can be seen in Figure S22, the isotope pattern of the experimentally observed peak at around *m/z* 2554 Da matched better with [PdHCu₁₁{S₂P(OⁱPr)₂}(C≡CPh)₄] than [PdDCu₁₁{S₂P(OⁱPr)₂}(C≡CPh)₄], suggesting that the hydride remained intact during the HER process. In other words, *it is here to stabilize the Pd-containing neutral cluster and does not participate in the HER pathway.*

To gain further insight into the origin of the high HER activity of **PdHCu₁₁**, the hydrogen adsorption energies (ΔG_H) on the **PdHCu₁₁'** and **PdHCu₁₂'** nanocluster models were computed under the conditions of a standard hydrogen electrode at zero overpotential, according to the approach proposed by Nørskov *et al.*³⁶ Square wave voltammograms in Figure S23 show that the charge states of **PdHCu₁₁** and **PdHCu₁₂** nanoclusters are zero at potentials where HER studies were conducted in Figure 4a and thus the computations were conducted based on neutral nanoclusters for these model nanoclusters. A moderate energy barrier of 1.08 eV was found for **PdHCu₁₁'** (Figure S24a), which can explain the remarkable HER activity of **PdHCu₁₁**, although it is somewhat higher than expected. Interestingly, the energy barrier found for **PdHCu₁₂'** (0.95 eV) is of the same order of magnitude, despite the much less efficient HER activity of **PdHCu₁₂**. These values barely change when solvent (water) effects are included. We note that the Nørskov model is solely based on thermochemistry, neglecting other contributions such as kinetic barriers.³⁶ Therefore, compared with **PdHCu₁₂'** having a similar energy barrier, the dramatically enhanced HER activity observed for the **PdHCu₁₁** nanocluster can be ascribed to its unique structure. That is, the presence of a vacancy in **PdHCu₁₁'** allows an easy approach of the added hydrogen to Pd, whereas, in the **PdHCu₁₂'** nanocluster, its penetration inside the closed copper cage likely requires substantial activation energy, which is not considered in the ΔG_H calculation.

Of note, the added hydrogen was found to lie well inside the vacancy created by the missing cuboctahedron vertex in the optimized structure of [**PdHCu₁₁-H'**] (Figure S24b). The adsorbed H binds at the PdCu₈Cu₉ triangle with Pd-H = 1.696 Å and Cu-H(av) = 1.744 Å. Besides this addition, the cluster molecular framework remains the same. This result clearly corroborates the structural effect of **PdHCu₁₁** having a defective cuboctahedron in the HER process. That is, the adsorbed H penetrates the vertex-missing cuboctahedron shell of **PdHCu₁₁** and directly interacts with the Pd dopant, as well as, in a weaker way, with three Cu atoms. Thus, it can be concluded that the defective Cu₁₁ framework of **PdHCu₁₁** participates in the HER process by stabilizing the reaction intermediate as well as providing the reaction site. By contrast, the interaction between the adsorbed H and the central Pd dopant is kinetically blocked in the complete cuboctahedron Cu₁₂ or bicapped icosahedral Cu₁₄ cages.

Conclusion

Herein we report the synthesis and full characterizations of two atom-precise, hydride-containing 2-electron palladium/copper superatomic alloys co-protected by alkynyl and dithiophosphate ligands. The **PdHCu₁₁** kernel consists of a Pd(0) atom encapsulated within a Cu₁₁ cage describing a vertex-missing cuboctahedron. **PdHCu₁₂** can be viewed as a complete

cuboctahedron Pd-centered Cu₁₂. The hydride in both **PdHCu₁₁** and **PdHCu₁₂** is found to locate within a PdCu₃ tetrahedron and is rather strongly bonded to Pd. DFT calculations indicate that both **PdHCu₁₁** and **PdHCu₁₂** are a 2-e superatom with 1S² configuration, similarly to the fully cuboctahedral [MCu₁₂{dtc/dtp}₆(C≡CPh)₆]⁺ (M = Cu, Ag, Au) clusters.^{24,25} This electron count parentage is reminiscent of the well-known closo/nido relationship in clusters obeying the Wade-Mingos rules.²⁸ However, due to the presence of nearly linear H-Pd-C bonding, **PdHCu₁₁** and **PdHCu₁₂** are axially distorted superatoms. Calculations indicate that the electron of the encapsulated hydrogen atom should be included in the superatomic count, despite the weak participation of its 1s AO to the superatomic orbitals. Rather, the 1s(H) AO interacts preferentially with a 4d(Pd) orbital to make a Pd-H σ bonding.

The unique structural feature of **PdHCu₁₁** is explored as an effective electrocatalyst for the hydrogen evolution reaction, which shows high performance in the HER activity. The HER activity of the **PdHCu₁₁** exhibits an onset potential of –0.05 V at a current density of –10 mA cm^{–2} and the Tafel slope of 40 mV dec^{–1}. The **PdHCu₁₁** displayed the faradaic efficiency for H₂ production at about 96 % at –0.05 V and increased to over 99 % when the onset potential was –0.10 V. It afforded the TOF more than 250 s^{–1} (at overpotential 0.1 V) and showed high durability during 1000 cycles. The calculations suggest that the “adsorbed” hydrogen takes advantage of the cluster vacancy and of the affinity of Pd for hydrogen to bind the central metal atom and leave its adsorption site as dihydrogen upon the entry of a second H atom. Thus, the encapsulated hydride is not directly involved in the HER mechanism. It is there to stabilize a Pd-containing neutral cluster which possesses a large vacancy allowing the approach of, for example, the adsorbed H. This discovery may give guidelines towards the correlation between the catalyst structure and HER activity.

Acknowledgements

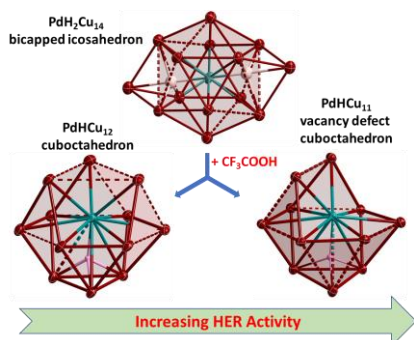
This work was supported by the National Science and Technology Council of Taiwan (111-2123-M-259-002), the GENCI computing resource (grant A0090807367), the National Research Foundation of Korea grants (NRF-2022R1A2C3003610 and Carbon-to-X Project No. 2020M3H7A1096388), and the Instrumentation Center of National Taiwan Normal University (NSTC 111-2731-M-003-001). HL thanks the China Scholarship Council for a PhD grant.

Keywords: Palladium • copper • hydride • hydrogen evolution reaction • electrocatalysts

- [1] R. Jana, A. Bhim, P. Bothra, B. K. Pati, S. C. Peter, *ChemSusChem.*, **2016**, *9*, 2922-2927.
- [2] J. Zhu, L. Hu, P. Zhao, L. Y. S. Lee, K.-Y. Wong, *Chem. Rev.*, **2020**, *120*, 851-918.
- [3] C. Li, J.-B. Baek, *ACS Omega*, **2020**, *5*, 31-40.
- [4] S. Sarkar, S. C. Peter, *Inorg. Chem. Front.*, **2018**, *5*, 2060-2080.
- [5] M. A. Ehsan, M. H. Suliman, A. Rehman, A. B. Hakeem, Z. H. Yamani, M. Qamar, *New J. Chem.*, **2020**, *44*, 7795-7801.
- [6] Q. Yao, K. Yan, W. Zhu, Y. Zheng, *J. Phys. Chem. Lett.*, **2021**, *12*, 7373-7378.
- [7] M. H. Naveen, Y. Huang, S. B. Kantharajappa, K.-D. Seo, D.-S. Park, Y.-B. Shim, *ACS Appl. Energy Mater.*, **2021**, *4*, 575-585.

- [8] B. D. Adams, A. Chen, *Materials Today*, **2011**, *14*, 282-289.
- [9] X. Zhang, D. Wu and D. Cheng, *Electrochimica Acta*, **2017**, *246*, 572-579.
- [10] D. Wu, H. Xu, D. Cao, A. Fisher, Y. Gao, D. Cheng, *Nanotechnology*, **2016**, *27*, 495403.
- [11] X. Yang, W. Xu, S. Cao, S. Zhu, Y. Liang, Z. Cui, X. Yang, Z. Li, S. Wu, A. Inoue, L. Chen, *Applied Catalysis B: Environmental*, **2019**, *246*, 156-165.
- [12] J. Li, F. Li, S.-X. Guo, J. Zhang, J. Ma, *Applied Materials & Interfaces*, **2017**, *9*, 8151-8160.
- [13] B. Zhang, H. Zhu, M. Zou, X. Liu, H. Yang, M. Zhang, W. Wu, J. Yao, M. Du, *J Mater Sci.*, **2017**, *52*, 8207-8218.
- [14] K. Kwak, W. Choi, Q. Tang, M. Kim, Y. Lee, D.-e. Jiang, D. A. Lee, *Nat. Commun.*, **2017**, *8*, 14723.
- [15] A. J. Edwards, R. S. Dhayal, P.-K. Liao, J.-H. Liao, M.-H. Chiang, R. O. Piltz, S. Kahlal, J.-Y. Saillard, C. W. Liu, *Angew. Chem. Int. Ed.*, **2014**, *53*, 7214-7218.
- [16] R. S. Dhayal, J.-H. Liao, Y.-R. Lin, P.-K. Liao, S. Kahlal, J.-Y. Saillard, C. W. Liu, *J. Am. Chem. Soc.*, **2013**, *135*, 4704-4707.
- [17] K. K. Chakrahari, R. P. B. Silalahi, T.-H. Chiu, X. Wang, N. Azrou, S. Kahlal, Y.-C. Liu, M.-H. Chiang, J.-Y. Saillard, C. W. Liu, *Angew. Chem. Int. Ed.*, **2019**, *58*, 4943-4947.
- [18] T.-H. Chiu, J.-H. Liao, F. Gam, Y.-Y. Wu, X. Wang, S. Kahlal, J.-Y. Saillard, C. W. Liu, *J. Am. Chem. Soc.*, **2022**, *144*, 23, 10599-1060.
- [19] H. Yi, S. M. Han, S. Song, M. Kim, E. Sim, D. Lee, *Ang. Chem. Int. Ed.*, **2021**, *60*, 22293-22300.
- [20] H. Hirai, S. Takano, T. Tsukuda, *ACS Omega*, **2019**, *4*, 7070-7075.
- [21] R. P. B. Silalahi, G.-R. Huang, J.-H. Liao, T.-H. Chiu, K. K. Chakrahari, X. Wang, J. Cartron, S. Kahlal, J.-Y. Saillard, C. W. Liu, *Inorg. Chem.*, **2020**, *59*, 2536-2547.
- [22] R. P. B. Silalahi, Q. Wang, J.-H. Liao, T.-H. Chiu, Y.-Y. Wu, X. Wang, S. Kahlal, J.-Y. Saillard, C. W. Liu, *Angew. Chem. Int. Ed.*, **2022**, *61*, e202113266.
- [23] W. E. van Zyl, C. W. Liu, *Chem. Eur. J.*, **2022**, *28*, e202104241.
- [24] R. P. B. Silalahi, T.-H. Chiu, J.-H. Kao, C.-Y. Wu, C.-W. Yin, Y.-C. Liu, Y. J. Chen, J.-Y. Saillard, M.-H. Chiang, C. W. Liu, *Inorg. Chem.*, **2021**, *60*, 10799-10807.
- [25] R. P. B. Silalahi, K. K. Chakrahari, J.-H. Liao, S. Kahlal, Y.-C. Liu, M.-H. Chiang, J.-Y. Saillard, C. W. Liu, *Chem. Asian J.*, **2018**, *13*, 500-504.
- [26] A. Chen, X. Kang, W. Du, S. Wang, M. Zhu, *J. Phys. Chem. Lett.*, **2019**, *10*, 6124-6128.
- [27] S. Takano, S. Hasegawa, M. Suyama, T. Tsukuda, *Acc. Chem. Res.*, **2018**, *51*, 12, 3074-3083.
- [28] D. M. P. Mingos, D. J. Wales, Englewood Cliffs, N.J. *Introduction to cluster chemistry*, Prentice Hall, **1990**.
- [29] T. Shinagawa, A. T. Garcia-Esparze, K. Takanabe, *Sci. Rep.*, **2015**, *5*, 13801.
- [30] Y. Du, J. Xiang, K. Ni, Y. Yun, G. Sun, X. Yuan, H. Sheng, Y. Zhu, M. Zhu, *Inorg. Chem. Front*, **2018**, *5*, 2948-2954.
- [31] Y. Li, S. Li, A. V. Nagarajan, Z. Liu, S. Nevins, Y. Song, G. Mpourmpakis, R. Jin, *J. Am. Chem. Soc.*, **2021**, *143*, 11102-11108.
- [32] G. Ma, Y. Tang, L. Chen, L. Qin, Q. Shen, L. Wang, Z. Tang, *Eur. J. Inorg. Chem.*, **2022**, e202200176.
- [33] Y. Tang, F. Sun, X. Ma, L. Qin, G. Ma, Q. Tang, Z. Tang, *Dalton Trans.*, **2022**, *51*, 7845-7850.
- [34] W. Choi, G. Hu, K. Kwak, M. Kim, D.-e. Jiang, J.-P. Choi, D. Lee, *ACS Appl. Mater. Interfaces*, **2018**, *10*, 44645-44653.
- [35] Y. Jo, M. Choi, M. Kim, J. S. Yoo, W. Choi, D. Lee, *Bull. Korean Chem. Soc.*, **2021**, *42*, 1672-1677.
- [36] J. K. Nørskov, T. Bligaard, A. Logadottir, J. R. Kitchin, J. G. Chen, S. Pandelov, U. Stimming, *J. Electrochem. Soc.*, **2005**, *152*, J23-J26.
- [37] Deposition numbers 2215591 (for **1**) and 2215592 (for **2**) contain the supplementary crystallographic data for this paper. These data are provided free of charge by the joint Cambridge Crystallographic Data Centre and Fachinformationszentrum Karlsruhe [Access Structures](#) service.

Entry for the Table of Contents



The acid treatment in **PdH₂Cu₁₄** leads to the transformation of a bicapped icosahedral **Cu₁₄** core into an incomplete Cu₁₁ (in **PdH₂Cu₁₁**) and a Cu₁₂ (in **PdH₂Cu₁₂**) cuboctahedron, both of which are 2e superatoms. Electrochemical HER experiments indicate while **PdH₂Cu₁₁**, **PdH₂Cu₁₂**, and **PdH₂Cu₁₄** are active catalysts, the stability and efficiency of **PdH₂Cu₁₁** is much higher than those of **PdH₂Cu₁₂** and **PdH₂Cu₁₄**.